IEEE Access
Multidisciplinary | Rapid Review | Open Access Journal

Received 22 August 2022, accepted 5 September 2022, date of publication 8 September 2022, date of current version 20 September 2022.

*Digital Object Identifier 10.1109/ACCESS.2022.3205347*

RESEARCH ARTICLE

# Effect of Beam Angle of the Transmitting Antenna on Radio Wave Coverage in the Region Containing Tunnel Entrance

**ZHENYU ZHAO[1,2], JUNHONG WANG[1,2], (Senior Member, IEEE), AND WEIBIN HOU[3]**

[1]Key Laboratory of All Optical Network and Advanced Telecommunication Network of MOE, Beijing Jiaotong University, Beijing 100044, China
[2]Institute of Lightwave Technology, Beijing Jiaotong University, Beijing 100044, China
[3]China Academy of Information and Communications Technology, Beijing 100191, China

Corresponding author: Junhong Wang (wangjunh@bjtu.edu.cn)

This work was supported in part by the National Natural Science Foundation of China under Grant 62031004 and Grant 61871025, and in part by the Fundamental Research Funds for the Central Universities under Grant 2020JBZ103.

**ABSTRACT** Radio wave coverage in open-confined mixed space along the railway is studied in this paper. The space along the railway can be classified into three kinds of spaces, that are, open space, confined space and the open-confined mixed space. The open-confined mixed space locates between the open space and confined space. In order to reveal the radio wave coverage mechanism in the open-confined mixed space and find out the important influence factors, the influence of antenna gain, antenna position, tunnel cross-section shape, and beam angle on the radio wave coverage in the open-confined mixed space are studied. Considering the complexity of environment, the radio wave coverage is modeled by finite difference time domain method. The simulation results show that the radio wave coverage is sensitive to the beam angle of transmitting antenna. And the variation law of radio wave coverage with the beam angle shows a certain correlation with the transmitting antenna position and tunnel cross-section shape.

**INDEX TERMS** Tunnel environment, open-confined mixed space, radio wave coverage, transmitting antenna, beam angle.

## I. INTRODUCTION

With the rapid development of high-speed railway in the world, remarkable achievements have been made in railway science and technology. To meet the requirements of high-safety train control and high-capacity public communication, stable radio wave coverage along the railway must be provided. However, the complex environments affect the property of radio wave coverage significantly, especially for the environment with tunnel entrance. Therefore, the research on the effective coverage of radio wave in this kind of complex space is of great important.

The radio wave coverage along the railway has been studied for a long time [1], [2], [3], [4], and it can be modeled and predicted by measurements or by physics-based methods. Several measured works on radio wave coverage in open space along the railway have been published. In [5], the author investigates the cross-correlation characteristics of large-scale parameters (LSPs) and small-scale fading (SSF) for high-speed railway (HSR) multilink propagation scenarios, based on realistic measurements conducted on Beijing to Tianjin HSR line in China. In [6], measurements of received signal strength and power delay profiles are carried out in traditional train station and the HSR tunnel, and non-stationarity of the channel is analyzed. For the tunnel scene, there are also many measurement works having been carried out [7], [8], [9], [10], [11]. Among them, [7] conducts a series of measurements between 31.5–31.75 GHz with 250 MHz bandwidth in Seoul subway line 8 by Electronics and Telecommunications Research Institute (ETRI), and the signal-to-noise ratios (SNRs) and power delay profiles (PDPs) are studied. [8] conducts measurements in London Underground Subway to verify the validity of proposed optimization technique. At the same time, there are also some works focusing on the

The associate editor coordinating the review of this manuscript and approving it for publication was Shah Nawaz Burokur.

field measurement of radio waves in the open-confined mixed space. For example, [12] measures the wide-band parameters, such as root mean square (RMS) delay spread, coherence bandwidth, etc., in small passageway tunnels under nonline-of-sight (NLoS) conditions and studied how these parameters behave in the tunnel entrance, when the position of transmitting antenna changes. [13] studies the road-to-vehicle and vehicle-to-vehicle communication property in the tunnel entrance environment through the propagation measurement, and focuses on the transition effect in the tunnel entrance environment, when the train moving from outside into the tunnel. These measurement results can provide insights into the propagation characteristics of the studied channels, but it is time consuming and difficult to reveal the propagation mechanism.

For the physics-based methods, there are analytical approaches, such as waveguide theory [14], [15], and simulation techniques, such as vector parabolic equation (VPE) [16], [17], [18], ray tracing (RT) methods [19], [20], [21], and the finite-difference time-domain (FDTD) [22], [23]. Waveguide theory can be used to analyze the wave propagation characteristics in tunnels with regular cross sections effectively and accurately, however, it is not suitable for complex tunnel environments. The VPE method is efficient and suitable for large-scale environments, however, it is effective only for the propagation of paraxial waves; hence, the calculation accuracy of wave propagation near the transmitting antenna is not sufficient, especially for those cases that antenna pattern is not paraxial. Ray tracing technique is also implemented to simulate the railway scene, which is based on ray optics and the uniform theory of diffraction (UTD) [12], [24]. The principal of ray tracing method is based on the superposition of the reflected rays from reflecting surfaces to obtain the receiving field. Hence the accuracy of ray tracing method needs to be improved for the open-confined mixed space where lots of scattering and diffraction exist. FDTD method has higher accuracy in the analysis of radio wave coverage, but it requires large amount of computation and is time-consuming. Fortunately, with the development of computer technology and parallel computing technology based on message passing interface (MPI) method [25], [26], FDTD now can be used to simulate the wave propagation in large complex environments.

The available researches on radio wave coverage characteristics along the railway are mainly done for single environment, such as, single open space or single confined space. While for the open-confined mixed space, only some measurement results [12], [13] and a few studies of physics-based methods [24], [27] can be found. These studies on the radio wave coverage of open-confined mixed space show that the radio wave generated by the antenna outside the tunnel can meet the minimum receiving threshold requirements and realize the coverage of open-confined mixed space. However, how the antenna and environmental parameters affect the radio wave coverage in the mixed space and how to achieve a more uniform and stable radio wave coverage in the mixed space remains to be studied. On the one hand, in consideration of the complexity of the simulation scenario and the close relationship between radio wave coverage and antenna characteristics, this paper utilizes the FDTD method to analyze the influence of the antenna position, tunnel cross-section shape and beam angle on the radio wave coverage in the open-confined mixed space. On the other hand, parallel FDTD technology and coarse-fine mesh combined method are used to improve the simulation efficiency.

The simulation model of the open-confined mixed space is described in detail in Section II. The effects of antenna position and beam angle on radio wave coverage in two kinds of hybrid spaces, which are open space connected with rectangular tunnel and open space connected with arched tunnel, are presented in Section III and Section IV, respectively. Conclusions are summarized in Section V.

## II. SIMULATION MODEL AND FORMULATION

In this paper, considering the complexity of the simulation environment and the requirement of accuracy, FDTD method is applied to model radio wave propagation in the hybrid region with open space and confined space (tunnel). Meanwhile, to overcome the challenges of density mesh, fine FDTD meshes are only used in modeling the practical antenna structures and coarse meshes are used in modeling rest of the environment. As shown in Fig. 1, the sub-domain of antenna is simulated first with fine meshes, and the field in this sub-domain is then coupled into the outside environment with the help of equivalent electric and magnetic currents at the common boundary of the two sub-domains.

### A. MODELING OF YAGI-UDA ANTENNA

In railway scenes, Yagi-Uda antenna is widely used as transmitting antennas (Tx) due to their narrow beamwidth and high gain. In this paper, two kinds of Yagi-Uda antennas with different gains are selected as transmit antennas, respectively, one of which has a gain of 6.41 dBi and the other has a gain of 12 dBi. The radiation patterns of the two antennas working in the 900 MHz are shown in Fig. 2. For the application of coarse-fine mesh hybrid method, the sub-domain of antenna is simulated in free space with fine mesh, and the tangential electric and magnetic fields on the sub-domain boundary are stored. Then, these fields are converted into the tangential electric and magnetic currents on the environment sub-domain boundary by

$$\boldsymbol{J} = \hat{n} \times \boldsymbol{H}, \tag{1}$$

$$\boldsymbol{J}_s = \boldsymbol{E} \times \hat{n}, \tag{2}$$

where $\hat{n}$ is the normal vector of the equivalent surface, $\boldsymbol{E}$ and $\boldsymbol{H}$ are the stored tangential electric and magnetic fields on the sub-domain boundary, respectively. $\boldsymbol{J}$ and $\boldsymbol{J}_s$ are the equivalent tangential electric and magnetic currents on the environment sub-domain boundary, respectively. Consequently, the radiation field of the antenna is obtained by the equivalence principle.

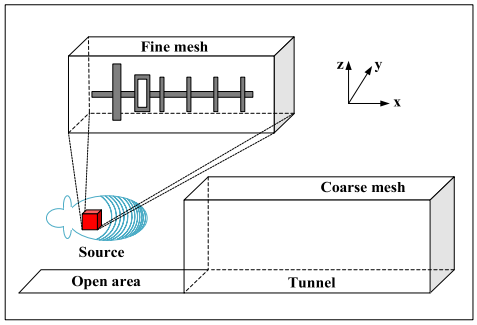


**FIGURE 1.** Description of the whole simulation area including antenna subdomain the environment.

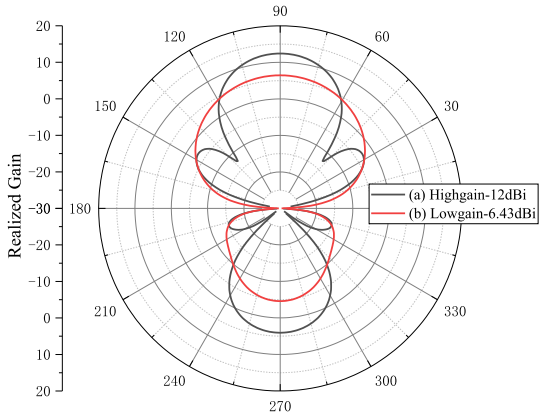


**FIGURE 2.** Radiation patterns of two Yagi-Uda antennas, (a) with high gain and (b) with low gain.

In this paper, the sizes of fine and coarse meshes are set to $\Delta x = \Delta y = \Delta z = 0.005$m and $\Delta x = \Delta y = \Delta z = 0.0333$m, respectively. Parallel MPI technique is applied in this paper to shorten iterative time. The parallel algorithm of FDTD utilizes a one-cell overlap region to exchange the information between adjacent sub-domains. In the algorithm, only the tangential magnetic fields are exchanged at each timestep.

### B. MODELING OF OPEN-CONFINED MIXED AREA

In this paper, the Yagi-Uda antenna is placed along $x$-axis in open space. The fine mesh numbers for simulating the antenna region are 300 × 200 × 300 cells, and the equivalent surface for output the tangential field component occupy 46, 31 and 46 coarse cells in $x$, $y$, and $z$ directions, respectively. For the total simulation environment, there are 1064 × 224 × 200 coarse mesh cells, which contain a 10-meter-long open area and a 25-meter-long tunnel. Two tunnels with different cross-sectional shapes are considered, namely rectangular tunnel and arched tunnel. The specific dimensions of rectangular tunnel and arched tunnel will be introduced in Section III and Section IV, respectively. In addition, the tunnel and open space in calculation region are extended to the perfectly matched layers (PML) to ensure that there is no reflected wave from the boundary, which simulates the case of an infinite environment. As shown in Fig. 3, the thicknesses of PML in $x$, $y$ and $z$ directions are set to 20 grids, respectively.

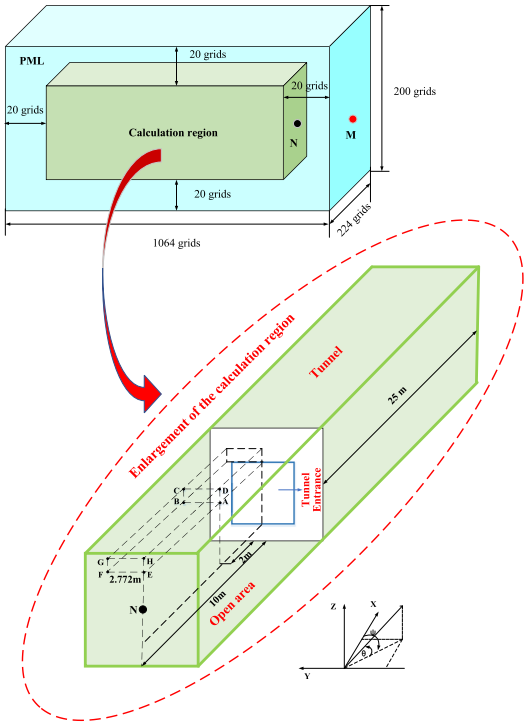


**FIGURE 3.** Diagram of the FDTD model for open-confined mixed space and the eight transmitting antenna positions.

### C. EVALUATION PARAMETERS FOR DIFFERENT SIMULATION CASES

As done by other literatures, the received power distribution in the environment is simulated and studied in this paper. To observe the impact of environment on radio wave coverage more intuitively, in addition to directly comparing the difference between the received power curves, this paper also uses the parameters, median field intensity (MFI) proposed in [28] and system field strength flatness factor (FLmax) proposed in [29], to evaluate the large-scale fading and small-scale fading characteristics of the radio wave coverage along the receiving path, respectively. For the simulation environment of this paper, the formula of MFI is expressed as

$$A_{sa} = \frac{1}{x_0}\int_0^{x_0} A_s(x)dx\,, \tag{3}$$

where $x_0$ is the length of the simulation path of whole environment (including open space and tunnel), $x$ is the position of the receiving point along the x-axis direction, and $A_s(x)$ is the local median electric field intensity at reception point $x$, which is represented by the average electric field of multiple equally-spaced sampling points around the reception point. To better reflect the local median received electric field, $A_s$ in this paper is calculated by taking the average of electric field values at total 11 points centered by the observing point. Therefore, the formula of $A_s$ is expressed as

$$A_s(x) = \frac{\sum_{n=-5}^{5} A(x + n \cdot \Delta_x)}{11}\,, \tag{4}$$

where $A$ is the actual received electric field at different sampling reception points. For FLmax, the formula is the same as given in [29].

## III. NUMERICAL RESULT OF RECTANGULAR TUNNEL AND ANALYSIS

This section aims to study the influence of Tx beam angle on the radio wave coverage in mixed space of open space connected with rectangular tunnel. The width and height of inner cross section of the considered rectangular tunnel are 5 m and 4 m, respectively. The relative dielectric constant and conductivity of the tunnel wall are set to 5 and 0.01 S/m, respectively. For a more comprehensive consideration, this section not only uses two kinds of Yagi-Uda antennas with different gain, but also places transmitting antenna in 8 different positions in open space. The model of considered open-confined mixed space and transmitting antenna positions are shown in Fig. 3. $\psi$ and $\theta$ in Fig. 3 represent the azimuthal and elevation angles, respectively.

In practice, there are many typical antenna layouts for radio wave coverage in the tunnel entrance and exit areas. In this paper, we consider the situation that the base station is mounted outside the tunnel, which receives and amplifies the signal from another far base antenna, and then radiates towards the tunnel entrance to cover the space where open area and tunnel are mixed. In Fig. 3, the letters A to H represent eight antenna positions we considered in this paper. Among them, the four positions from A to D are located at the same vertical plane with 2 m away from the tunnel entrance plane, and E to H are located 10 m from the tunnel entrance plane. The heights of positions of A, B, E and F are the same as tunnel height; the heights of positions of C, D, G and H are 1.32 m higher than the tunnel height. The center of the first layer grid of the calculation region in the $x$-direction is set as the origin, namely point N in Fig. 3. The position coordinates of points A to H are (8 m, 0 m, 2 m), (8 m, −2.772 m, 2 m), (8 m, −2.772 m, 3.32 m), (8 m, 0 m, 3.32 m), (0m, 0 m, 2 m), (0 m, −2.772 m, 2 m), (0 m, −2.772 m, 3.32 m), (0 m, 0 m, 3.32 m), respectively. The receiving antenna is located in the center of cross-section tunnel, and 3.2 m away from the ground. The receiving antenna records the electric fields when moving along the simulation distance (passing through both the open space and tunnel). To analyze the influence of the beam angles in azimuthal and elevation directions of the transmitting antenna on the radio wave coverage, five azimuthal angles and three elevation angles are considered for each antenna position.

### A. INFLUENCE OF THE AZIMUTHAL BEAM ANGLE OF LOW GAIN ANTENNA ON THE RADIO WAVE COVERAGE

This part presents the radio wave coverage results generated by low-gain Yagi-Uda antenna with different beam angles in azimuthal directions at different locations. Figures 4 (a)-(h) show the received power curves obtained when the beam direction of transmitting antenna changes in azimuthal direction at eight positions from A to H. The legends

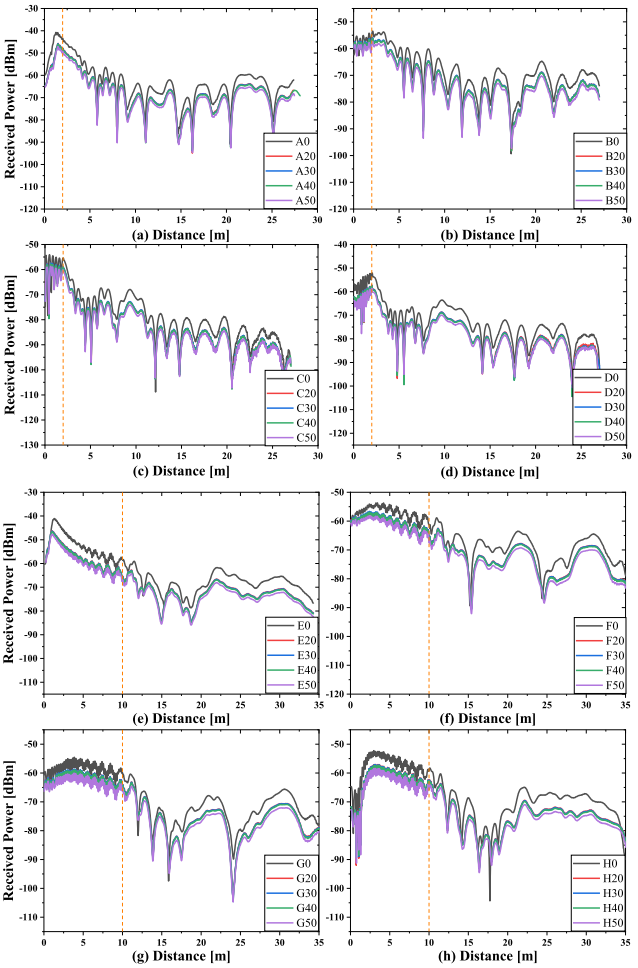


**FIGURE 4.** Simulated received power of low-gain Yagi antenna with 5 azimuthal beam angles at 8 positions: (a) position A, (b) position B, (c) position C, (d) position D, (e) position E, (f) position F, (g) position G, (h) position H.

A0, A20, …, A50 in Fig. 4(a) mean that the transmitting antenna is placed at position A and its beam is pointing to 0, 20, …, 50 degrees in the azimuthal plane. The legends in Figures 4 (b)-(h) have the similar explanation. The x-axis of figures represents the distances from the receiving points to the transmitting antenna. The orange demarcation lines in Fig. 4 represent the location of the tunnel entrance. The MFI and FLmax obtained in different cases are summarized in Figs. 5 and 6, respectively.

From Fig. 4, we can see that for the low gain Yagi-Uda antenna, when the azimuthal angle is switched from 0 to 20 degrees, the influence of the azimuthal angle on the radio wave coverage is the most obvious. The received power at 0 degree in azimuthal plane is significantly higher than that of 20 degrees. However, when the azimuthal angle is switched from 20 degrees to 40 degrees, the impact on the radio wave coverage is not so great, but the radio wave coverage is significantly reduced when beam angle is pointing at 50 degrees. It is also noted that the radio waves generated by the transmitting antennas located at position A-D, which are closer to

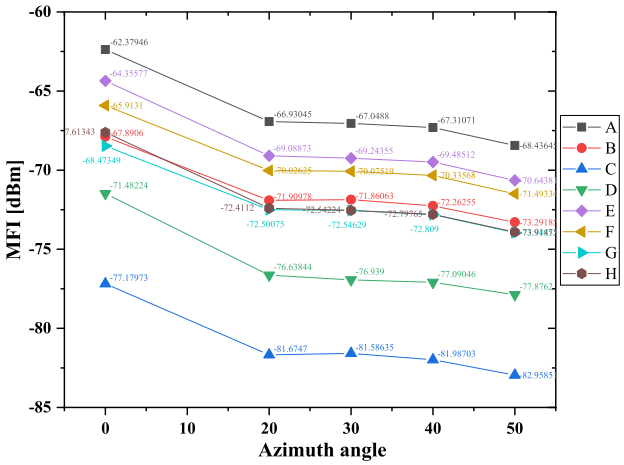


**FIGURE 5.** Results of median field intensity for low-gain Yagi antenna with different azimuthal beam angles at different positions.

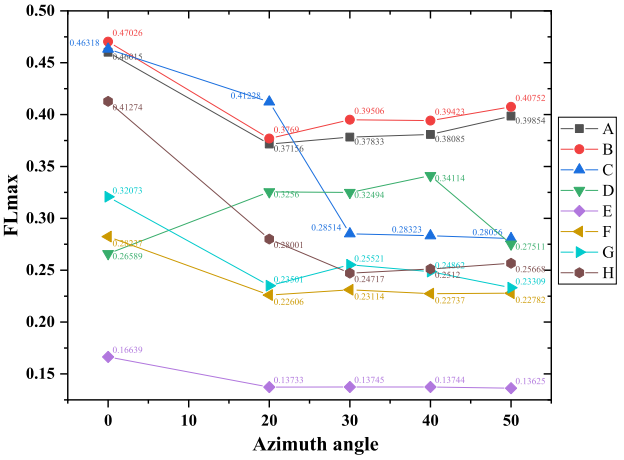


**FIGURE 6.** Results of flatness factor for low-gain Yagi antenna with different azimuthal beam angles at different positions.

the tunnel entrance, will experience rapid attenuation within three meters in the beginning of tunnel, after then the radio waves show regular attenuation caused by the tunnel waveguide effect. But the receiving power generated by the antennas located at E-H, attenuates smaller and slower when entering the tunnel. The reason for this phenomenon can be explained from the perspective of the reflection and diffraction. The total field received at the tunnel entrance is basically the superposition of the direct incident wave, multi-walls reflection wave and the diffraction wave from the corners of tunnel entrance. Using geometric ray tracing analysis, we can find that, for the case of transmitting antenna locating at distance of 10 m away from the tunnel entrance, the phase difference due to the path difference between different reflected wave and diffracted wave near the tunnel entrance changes slower than that of the case when transmitting antenna locating at 2 m from tunnel entrance. Thus, the fluctuation of the wave near the tunnel entrance for the 10 m case is smaller than that of 2 m case. In addition, the received electric field in the far-field region is proportional to $1/r$, where $r$ is the distance from the transmitting antenna to receiving point. Thus, for the case of transmitting antenna locating at 10 m away, the amplitude of the incident electric field near the tunnel entrance is smaller, and the attenuation speed of the received wave near the tunnel entrance is slower than that of the 2 m case.

From Fig. 5, we can see that for each position, the influence of azimuthal beam angle on the large-scale fading of radio wave is basically the same. However, from Fig. 6, it can be observed that the effect of azimuthal beam angle on the small-scale fading of radio coverage is related to the antenna position. In other words, we can properly adjust the azimuthal angle of transmitting antenna to reduce the small-scale fading effect of the radio wave generated by the antenna at a certain position. On the other hand, by comparing the results in Fig. 5, we can see that the MFI obtained by the antenna closer to the upper wall of tunnel is higher than that of antenna located far away from the upper wall, and this is true for 5 azimuthal beam angle cases. Therefore, the MFI generated by the antenna at position C is the smallest, because the radio wave generated by the antenna here is greatly affected by the reflection of the upper wall and side wall of the tunnel entrance, resulting in evanescence wave. By comparing the results in Fig. 6, we find that at every azimuth angle, the FLmax obtained by the four antennas far from the tunnel entrance is smaller than that obtained by the near four closer to the ground for all 5 azimuthal beams angle cases. Therefore, the antenna located at position E gets the smallest FLmax by virtue of the reason that the generated radio wave is less affected by the reflections from both the upper and side walls of the tunnel entrance. Finally, by comparing the results in Figs. 5 and 6, we can find that the distance between the antenna and the side wall of tunnel has no obvious effect on the radio wave coverage.

### B. INFLUENCE OF THE ELEVATION BEAM ANGLE OF LOW GAIN ANTENNA ON THE RADIO WAVE COVERAGE

The radio wave coverage results generated by low gain Yagi-Uda antenna with different beam angles in elevation direction are presented in this section. Figures 7 (a)-(h) show the obtained received power when the beam direction of transmitting antenna changes in elevation plane at eight positions from A to H. The legends A0, A15, A25 in Fig. 7 mean that the transmitting antenna is placed at position A and its beam is pointing to 0, $-15$, $-25$ degrees in the elevation plane. The legends in Figs. 7 (b)-(h) have the similar explanation. The median field strength and flatness factor values obtained in different cases are summarized in Fig. 8 and 9, respectively.

From Fig. 7, we can see that for the low-gain Yagi-Uda antenna, the influence of the beam angle in azimuthal direction on radio wave propagation is greater than that in elevation direction. The radio wave coverage generated by the antenna located higher than the upper wall of the tunnel is more sensitive to the change of beam angle in elevation direction. When the radio waves generated by the transmitting antennas with different elevation angles pass through the tunnel

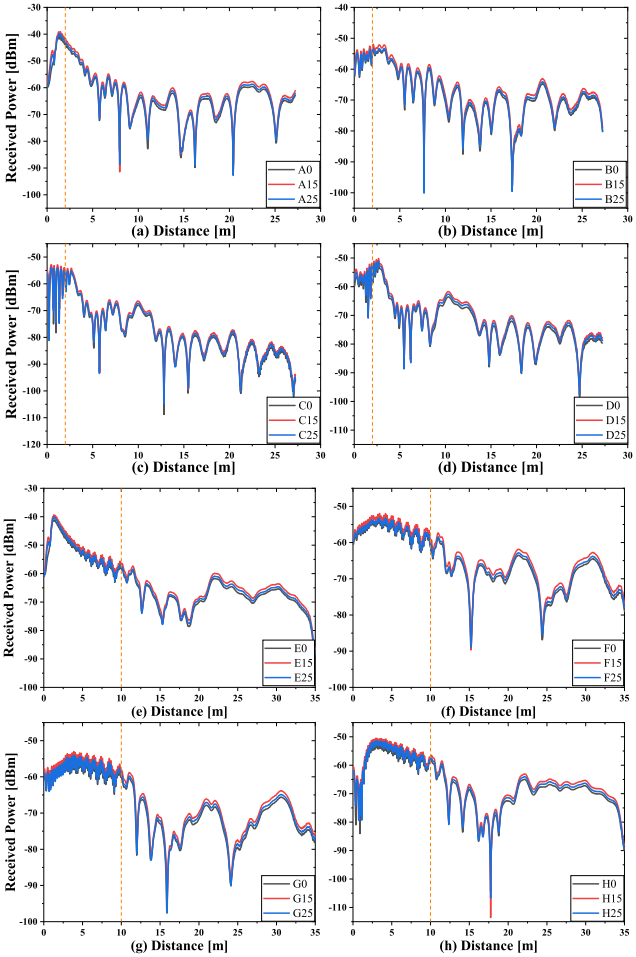


**FIGURE 7.** Simulated received power of low-gain Yagi antenna with 3 elevation beam angles at 8 positions: (a) position A, (b) position B, (c) position C, (d) position D, (e) position E, (f) position F, (g) position G, (h) position H.

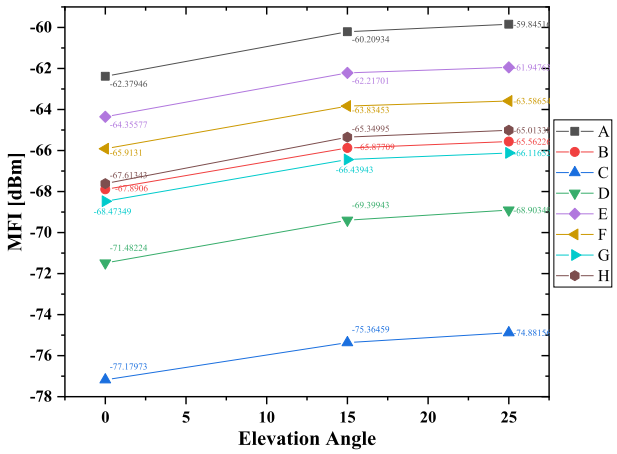


**FIGURE 8.** Results of median field intensity for low-gain Yagi antenna with different elevation beam angles at different positions.

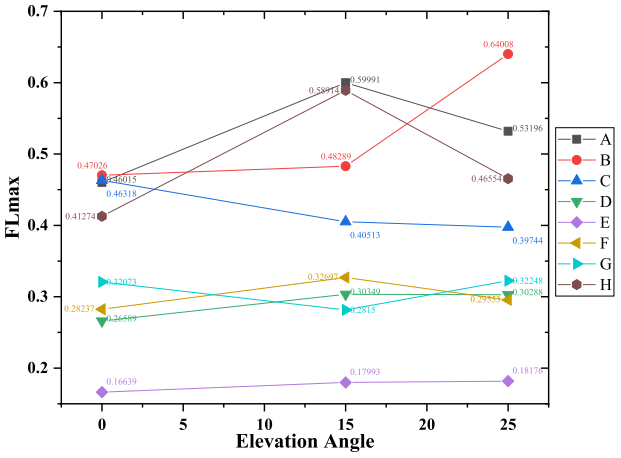


**FIGURE 9.** Results of flatness factor for low-gain Yagi antenna with different elevation beam angles at different positions.

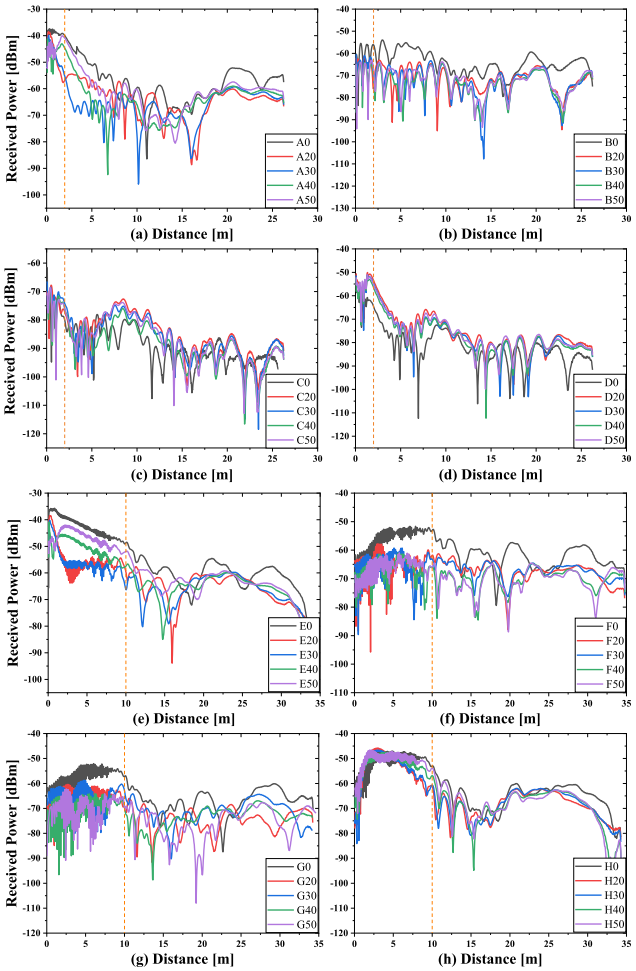


**FIGURE 10.** Simulated received power of high-gain Yagi antenna with 5 azimuthal beam angles at 8 positions: (a) position A, (b) position B, (c) position C, (d) position D, (e) position E, (f) position F, (g) position G, (h) position H.

entrance, they will undergo the similar attenuation process as that in the previous section, that is, the radio waves generated by the Tx closer to the tunnel entrance attenuate rapidly within a certain distance in the beginning of tunnel and then attenuate regularly. And comparing the in Figs. 8 and 9, it can be observed that the effect of the beam angle in elevation

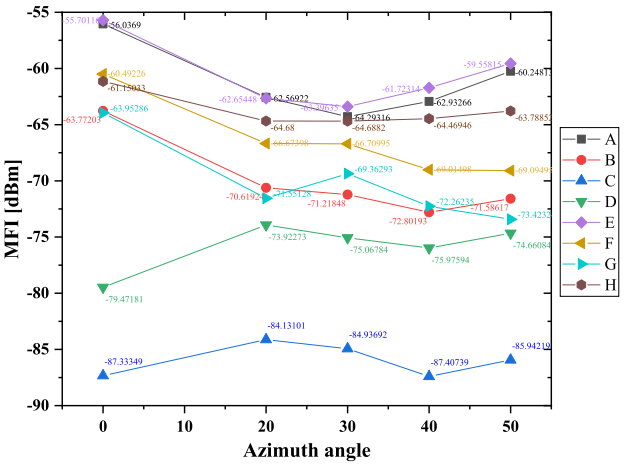


**FIGURE 11.** Results of median field intensity for high-gain Yagi antenna with different azimuthal beam angles at different positions.

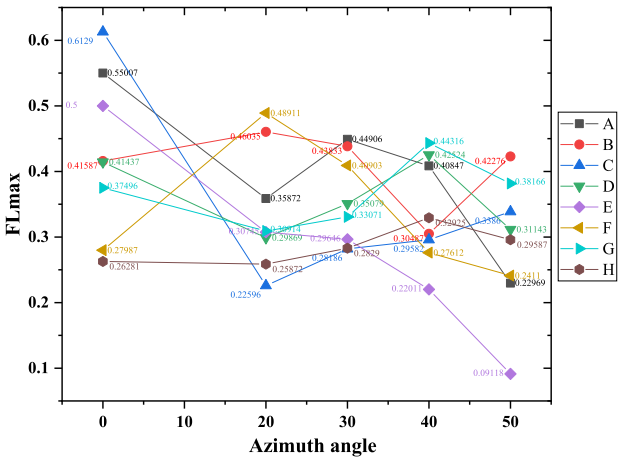


**FIGURE 12.** Results of flatness factor for high-gain Yagi antenna with different azimuthal beam angles at different positions.

directions on the large-scale fading is the same as that of the beam angle in azimuthal directions, that is, the effect of beam angle in elevation direction on the large-scale fading does not change with position. However, the effect of beam angle in elevation direction on the fast fading of radio wave coverage is related to the antenna position.

### C. INFLUENCE OF THE AZIMUTHAL BEAM ANGLE OF HIGH GAIN ANTENNA ON THE RADIO WAVE COVERAGE

Similarly, this part presents the radio wave coverage results of high gain Yagi-Uda antennas with different beam angles in azimuthal direction at different locations. Figures 10 (a)-(h) show the received power curves obtained when the beam direction of transmitting antenna changes in azimuthal direction at eight positions from A to H. The median field strength and flatness factor values obtained under different cases in this section are shown in Figs. 11 and 12, respectively.

From Fig. 10, we can see that compared with the low gain Yagi-Uda antenna, the radio wave coverage generated by the high gain Yagi-Uda antenna is more sensitive to the beam angles in azimuthal direction. For different beam angles in azimuthal direction, the radio wave coverages in the open space are different. From Figs. 11 and 12, we can see that for the high gain antenna, the influences of the beam angle in azimuthal direction on the large-scale fading and small-scale fading of radio wave coverage are both related to the position. The reason for this phenomenon is that the high gain Yagi antenna has a narrower beamwidth, so its radiation strength changes obviously with the beam angle. When the position of the antenna changes, the antenna radiation strength changes more dramatically in the direction of the straight-line path from the transmitting antenna to the receiving antenna, which leads to the greater impact on the radio wave coverage. On the other hand, it can be found that when the antenna is located closer to the tunnel entrance, the influence of beam angle in azimuthal direction on radio coverage is more sensitive with position. This can also be explained from the perspective of the diffraction theory. Because the transmitting antenna has a certain radiation beamwidth, so when the beam direction changes with a fixed angle, the variation of the incident field (as well as the diffraction field) on the tunnel entrance edges for the case of transmitting antenna locating at 2m will be faster than that of the case of 10m. Therefore, when the antenna beam angle changes, the radio waves generated by the transmitting antenna located closer to the tunnel entrance will be affected more significantly by the beam angle. Therefore, when considering the layout of transmitting antenna with high gain and narrow beamwidth, the beam angle in azimuthal direction should be adjusted properly when the position of antenna is changed.

### D. INFLUENCE OF THE ELEVATION BEAM ANGLE OF HIGH GAIN ANTENNA ON THE RADIO WAVE COVERAGE

The radio wave coverage results of high gain Yagi-Uda antenna with different beam angles in elevation direction at different locations are shown in this section. The received power curves obtained under different cases are shown in Fig. 13. The median field strength and flatness factor values are summarized in Figs. 14 and 15, respectively.

From Fig. 13, we can see that compared to the influence of beam angles in azimuthal direction discussed in last section, the influence of the beam angles in elevation direction of the high gain Yagi antenna on the radio wave coverage is not so severe, but it is still greater than the influence of the low-gain Yagi's beam angle in elevation direction. And for those antennas located lower than the upper wall of the tunnel, a better coverage can be obtained when the elevation angle is equal to 0 degrees, and the change of elevation angle in a small range has little effect on the radio wave coverage in the tunnel. However, for antennas located above the upper wall of the tunnel, beam angle in elevation direction has a more significant influence on the radio wave coverage of these antennas. In addition, it should be noted that when the antenna is located far away from the tunnel entrance, it is more difficult to optimize the radio wave coverage of

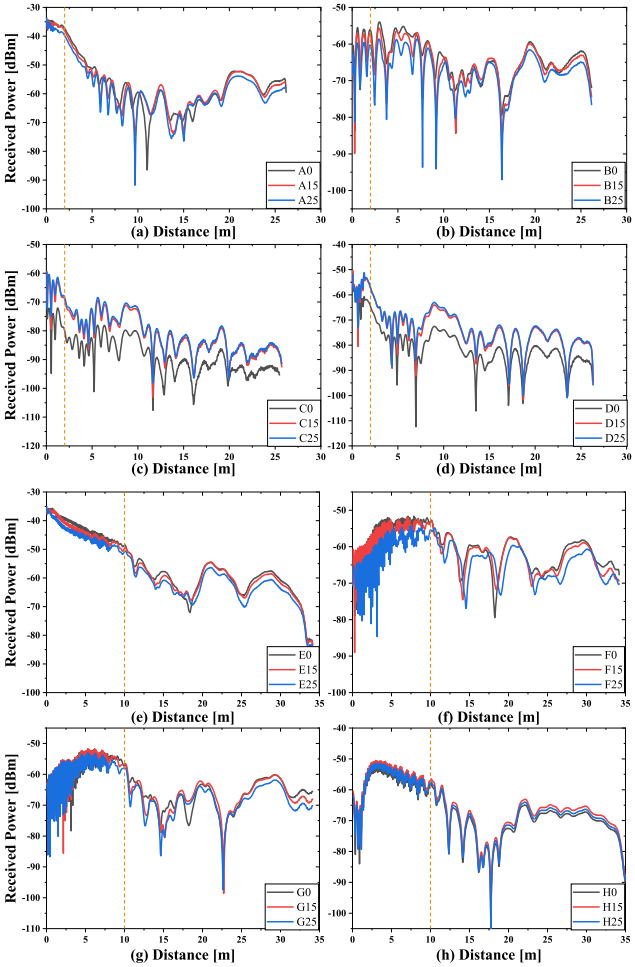


**FIGURE 13.** Simulated received power of high-gain Yagi antenna with 3 elevation beam angles at 8 positions: (a) position A, (b) position B, (c) position C, (d) position D, (e) position E, (f) position F, (g) position G, (h) position H.

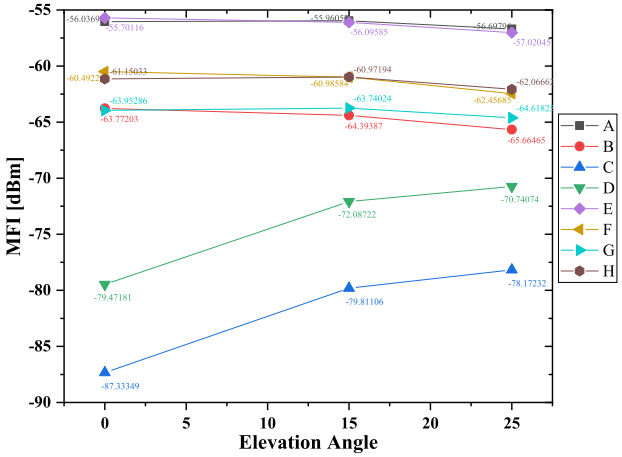


**FIGURE 14.** Results of median field intensity for high-gain Yagi antenna with different elevation beam angles at different positions.

tunnel by adjusting the beam angle in elevation direction. Secondly, by comparing the results in Figs. 14 and 15, we can see that the influence of beam angle in elevation direction

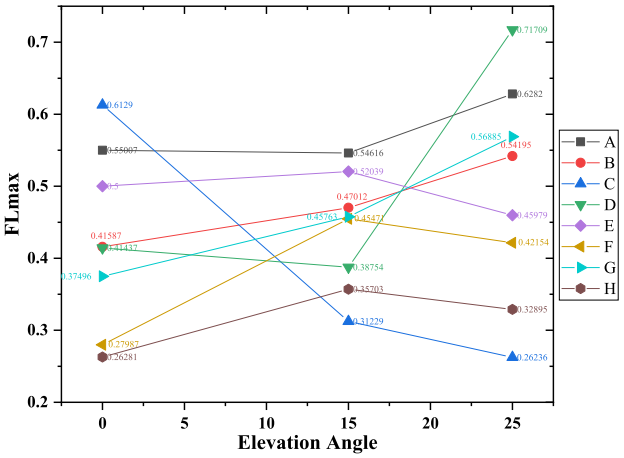


**FIGURE 15.** Results of flatness factor for high-gain Yagi antenna with different elevation beam angles at different positions.

on radio wave coverage is mainly on the small-scale fading. And as shown in Fig. 15, the influence of beam angle in elevation direction on small-scale fading is also affected by transmitting antenna position. Finally, we can conclude that for the high gain Yagi-Uda antenna, antenna position has more obvious effect on radio wave coverage than beam angle in elevation direction.

## IV. NUMERICAL RESULT OF ARCHED TUNNEL AND ANALYSIS

This section aims to study the influence of Tx beam angle on the radio wave coverage in mixed space of open space connected with an arched tunnel. In order to be more practical, a train is added to the simulation scene in this section. The schematic diagram of considered arched tunnel and train are shown in Fig. 16. For considered arched tunnel, $l$ is 25 m, $h$ is 4 m and $w$ is 3 m. The size of the train considered refers to the size of the actual freight train section, where $l_t$ is 25 m, $h_t$ is 2.8 m, and $w_t$ is 2.8 m. The train is located at the open-confined mixed space and the head of the train is located at a distance of $d$ from the origin, $d = 1.32$m. From the simulation conclusion of Section III, it can be found that the effect of high gain antenna beam angle variation on mixed space radio wave coverage is greater than that of low gain antenna, and the closer the transmitting antenna is located to the tunnel entrance, the more obvious the effect is. Therefore, in this section, we only study the effect of beam angle on radio wave coverage of mixed space when the high gain Yagi-Uda antenna is located at positions A, B, C and D in Fig. 3, respectively.

### A. INFLUENCE OF THE AZIMUTHAL BEAM ANGLE OF HIGH GAIN ANTENNA ON THE RADIO WAVE COVERAGE

For the open-confined mixed space in Fig. 16, the received power curves obtained for different azimuth angle cases are shown in Fig. 17. The MFI and FLmax obtained in different cases are summarized in Figs. 18 and 19 to evaluate the

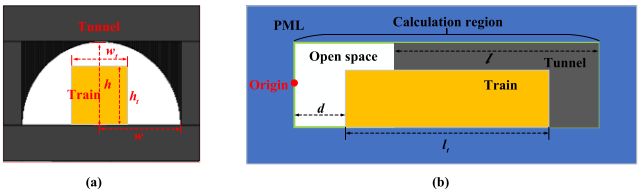


**FIGURE 16.** Diagram of the FDTD model for the scene where open space connected arched tunnel. (a) Left view of simulation model, (b) side view of simulation model.

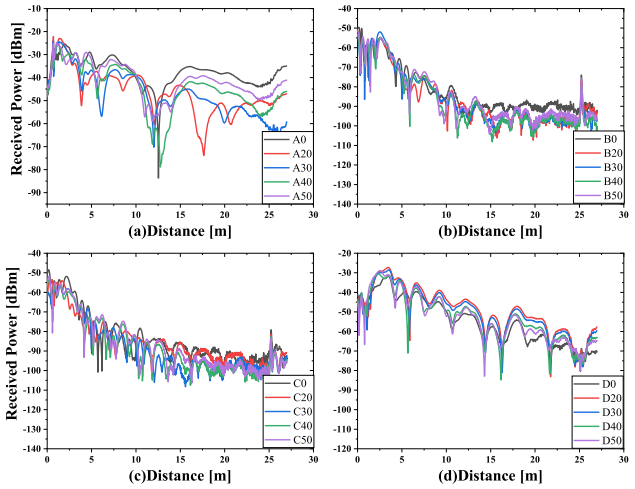


**FIGURE 17.** Simulated received power of high-gain Yagi antenna with 5 azimuthal beam angles at 4 positions: (a) position A, (b) position B, (c) position C, (d) position D.

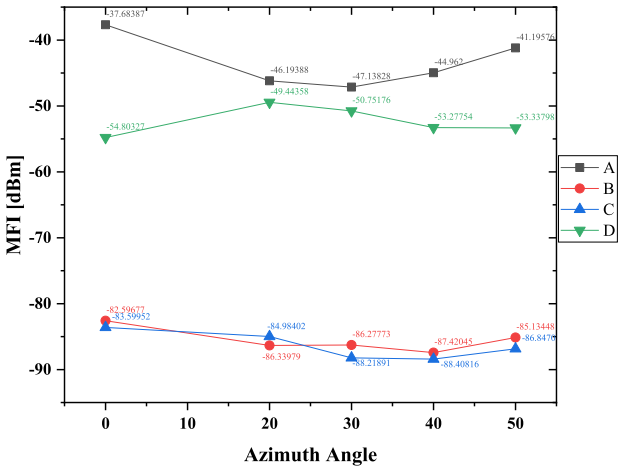


**FIGURE 18.** Results of median field intensity for high-gain Yagi antenna with different azimuthal beam angles at different positions.

large-scale fading and small-scale fading characteristics of the received power, respectively.

Compared with the received power curves in Section III, it can be found that the received power passing through the arched tunnel entrance does not vary significantly as that passing through the rectangular tunnel entrance. There are two main reasons for this phenomenon. One is that the cross-sectional area of the arch tunnel considered in

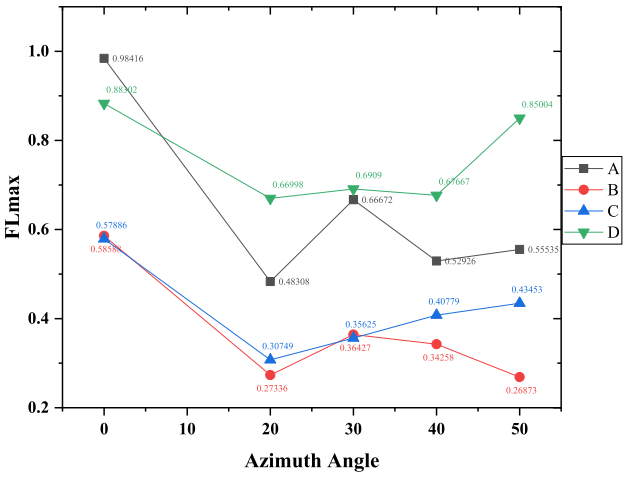


**FIGURE 19.** Results of flatness factor for high-gain Yagi antenna with different azimuthal beam angles at different positions.

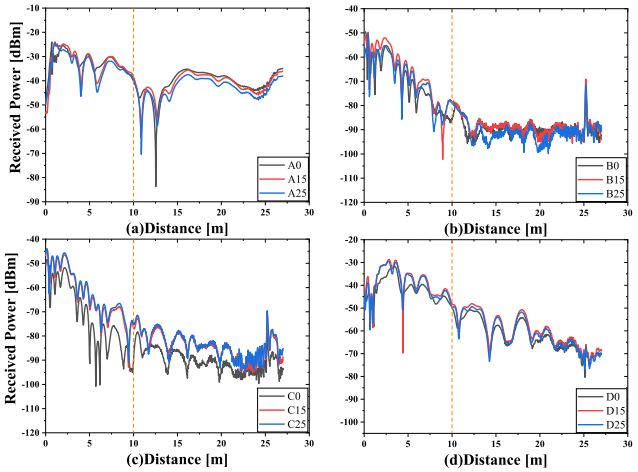


**FIGURE 20.** Simulated received power of high-gain Yagi antenna with5 elevation beam angles at 4 positions: (a) position A, (b) position B, (c) position C, (d) position D.

this section is larger than that of the rectangular tunnel in Section III, so the attenuation rate of radio waves in the arched tunnel can be smaller [30]; Secondly, the depolarization effect is more obvious in the arched tunnel, which results in a smaller number of polarization-matched reflection paths being received at the receiving antenna of the arched tunnel compared to the rectangular tunnel. In addition, the received. power in arched tunnel is more sensitive to the change of azimuth angle, especially the small-scale fading is obviously affected by the azimuth angle. As the Tx gets closer to the tunnel entrance, the influence of its azimuth angle on the generated radio waves becomes obvious.

### *B. INFLUENCE OF THE ELEVATION BEAM ANGLE OF HIGH GAIN ANTENNA ON THE RADIO WAVE COVERAGE*

For the open-confined mixed space in Fig. 16, the received power curves obtained for different elevation angle cases are shown in Fig. 20. The MFI and FLmax obtained in different cases are summarized in Figs. 21 and 22, respectively.

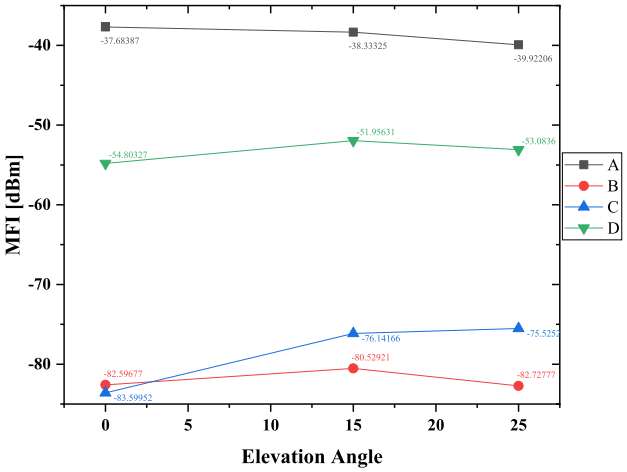


**FIGURE 21.** Results of median field intensity for high-gain Yagi antenna with different elevation beam angles at different positions.

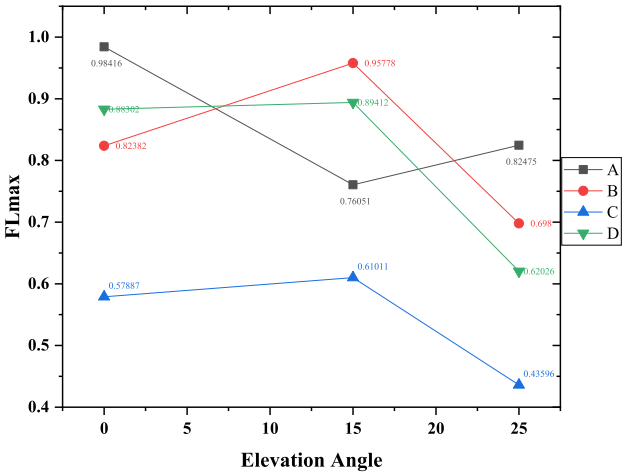


**FIGURE 22.** Results of flatness factor for high-gain Yagi antenna with different elevation beam angles at different position.

Compared with the simulation results of rectangular tunnel, the change of elevation angle has less influence on the radio wave coverage in the arched tunnel. At the same time, the influence of the change of elevation angles on the radio wave coverage in the arched tunnel is less than that caused by the change of azimuth angle. However, for the antenna located at the non-direct viewing position of the tunnel entrance (such as position B and C), the influence of elevation angle is more obvious. In these positions, the average received power can be increased by 3 dB by adjusting the elevation angle. Based on the simulation of all positions, an elevation angle of 15 degrees is a good choice, which ensures that the direct path experiences fewer reflections and avoids the absorption of electromagnetic waves by the upper tunnel wall.

## V. CONCLUSION

In this paper, the effects of beam angle, antenna position, antenna gain and tunnel cross-section shape on the radio wave coverage of open-confined space were simulated and compared. Simulation results show that the closer the antenna is to the tunnel entrance, the more severe fading of the received power will be experienced when passing through the tunnel entrance, and more deep fading points will be generated in the tunnel. When receiving antenna enters the arched tunnel entrance, the loss caused by scenario conversion is smaller than that of the rectangular tunnel. Meanwhile, the simulation results show that the effect of antenna beam angle on radio wave coverage in open-confined mixed space exhibits different laws for different antenna positions, antenna gains and tunnel cross-section shapes. The radio wave coverage generated by the high gain antenna closer to the arched tunnel entrance is more sensitive to the change of antenna beam angle. Therefore, when installing antenna equipment in open-confined mixed space, the antenna beam angle should be comprehensively considered in combination with antenna position, antenna gain and tunnel shape. From the simulation results, the case for azimuth angle of the antenna set parallel to tunnel axis and elevation angle set to 15 degrees downward is a relatively good choice.

## REFERENCES

[1] J. Lu, X. Chen, S. Liu, and P. Fan, "Location-aware ICI reduction in MIMO-OFDM downlinks for high-speed railway communication systems," *IEEE Trans. Veh. Technol.*, vol. 67, no. 4, pp. 2958–2972, Apr. 2018.

[2] Y. Lu, K. Xiong, P. Fan, and Z. Zhong, "Optimal multicell coordinated beamforming for downlink high-speed railway communications," *IEEE Trans. Veh. Technol.*, vol. 66, no. 10, pp. 9603–9608, Oct. 2017.

[3] J. Farooq and J. Soler, "Radio communication for communications-based train control (CBTC): A tutorial and survey," *IEEE Commun. Surveys Tuts.*, vol. 19, no. 3, pp. 1377–1402, 3rd Quart. 2017.

[4] B. Ai, A. F. Molisch, M. Rupp, and Z. D. Zhong, "5G key technologies for smart railways," *Proc. IEEE*, vol. 108, no. 6, pp. 856–893, Jun. 2020.

[5] T. Zhou, C. Tao, L. Liu, and K. Liu, "Investigation of cross-correlation characteristics for multi-link channels in high-speed railway scenarios," *China Commun.*, vol. 15, no. 8, pp. 108–117, Aug. 2018.

[6] D. Yu, G. Yue, N. Wei, L. Yang, H. Tan, D. Liang, and Y. Gong, "Empirical study on directional millimeter-wave propagation in railway communications between train and trackside," *IEEE J. Sel. Areas Commun.*, vol. 38, no. 12, pp. 2931–2945, Jun. 2020.

[7] K. Guan, B. Ai, B. Peng, D. He, G. Li, J. Yang, Z. Zhong, and T. Kürner, "Towards realistic high-speed train channels at 5G millimeter-wave band—Part II: Case study for paradigm implementation," *IEEE Trans. Veh. Technol.*, vol. 67, no. 10, pp. 9129–9144, Oct. 2018.

[8] X. Zhang, A. Ludwig, N. Sood, and C. D. Sarris, "Physics-based optimization of access point placement for train communication systems," *IEEE Trans. Intell. Transp. Syst.*, vol. 19, no. 9, pp. 3028–3038, Sep. 2018.

[9] T. Zhou, H. Li, R. Sun, Y. Wang, L. Liu, and C. Tao, "Simulation and analysis of propagation characteristics for tunnel train-ground communications at 1.4 and 40 GHz," *IEEE Access*, vol. 7, pp. 105123–105131, 2019.

[10] G. Yue, D. Yu, H. Qiu, K. Guan, L. Yang, and Q. Lv, "Measurements and ray tracing simulations for non-line-of-sight millimeter-wave channels in a confined corridor environment," *IEEE Access*, vol. 7, pp. 85066–85081, 2019.

[11] D. He, B. Ai, K. Guan, Z. Zhong, B. Hui, J. Kim, H. Chung, and I. Kim, "Channel measurement, simulation, and analysis for high-speed railway communications in 5G millimeter-wave band," *IEEE Trans. Intell. Transp. Syst.*, vol. 19, no. 10, pp. 3144–3158, Oct. 2018.

[12] J.-M. Molina-Garcia-Pardo, J.-V. Rodriguez, and L. Juan-Llácer, "Wideband measurements and characterization at 2.1 GHz while entering in a small tunnel," *IEEE Trans. Veh. Technol.*, vol. 53, no. 6, pp. 1794–1799, Nov. 2004.

[13] A. V. B. da Silva and M. Nakagawa, "Radio wave propagation measurements in tunnel entrance environment for intelligent transportation systems applications," in *Proc. IEEE Intell. Transp. Syst.*, Oakland, CA, USA, Aug. 2001, pp. 883–888.

[14] D. G. Dudley, M. Lienard, S. F. Mahmoud, and P. Degauque, "Wireless propagation in tunnels," *IEEE Antennas Propag. Mag.*, vol. 49, no. 2, pp. 11–26, Apr. 2007.
[15] X. Zhang and C. D. Sarris, "Vector parabolic equation-based derivation of rectangular waveguide surrogate models of arched tunnels," *IEEE Trans. Antennas Propag.*, vol. 66, no. 3, pp. 1392–1403, Mar. 2018.
[16] P. Bernardi, D. Caratelli, R. Cicchetti, V. Schena, and O. Testa, "A numerical scheme for the solution of the vector parabolic equation governing the radio wave propagation in straight and curved rectangular tunnels," *IEEE Trans. Antennas Propag.*, vol. 57, no. 10, pp. 3249–3257, Oct. 2009.
[17] X. Zhang and C. D. Sarris, "Statistical modeling of electromagnetic wave propagation in tunnels with rough walls using the vector parabolic equation method," *IEEE Trans. Antennas Propag.*, vol. 67, no. 4, pp. 2645–2654, Apr. 2019.
[18] X. Zhang, N. Sood, J. K. Siu, and C. D. Sarris, "A hybrid ray-tracing/vector parabolic equation method for propagation modeling in train communication channels," *IEEE Trans. Antennas Propag.*, vol. 64, no. 5, pp. 1840–1849, May 2016.
[19] D. Didascalou, T. M. Schafer, F. Weinmann, and W. Wiesbeck, "Ray-density normalization for ray-optical wave propagation modeling in arbitrarily shaped tunnels," *IEEE Trans. Antennas Propag.*, vol. 48, no. 9, pp. 1316–1325, Sep. 2000.
[20] N. Sood and C. D. Sarris, "Enabling accurate propagation modeling of complex tunnel geometries with ray-tracing," in *Proc. IEEE APS/URSI Int. Symp.*, Jul. 2017, pp. 1827–1828.
[21] D. Li and J. Wang, "Effect of antenna parameters on the field coverage in tunnel environments," *IEEE J. Antennas Propag.*, vol. 2016, no. 2, pp. 1–10, May 2016.
[22] D. Li, J. Wang, G. Tian, J. Zhou, and X. Lv, "An efficient algorithm based on the equivalence principle and FDTD for wave propagation prediction in tunnels," in *Proc. Int. Appl. Comput. Electromagn. Soc. Symp.-China (ACES)*, Jul. 2018, pp. 1–2.
[23] M. M. Rana and A. S. Mohan, "Segmented-locally-one-dimensional-FDTD method for EM propagation inside large complex tunnel environments," *IEEE Trans. Magn.*, vol. 48, no. 2, pp. 223–226, Feb. 2012.
[24] D. Di Napoli, F. Ferrara, C. Gennarelli, and G. Riccio, "A UAPO based model for predicting the field propagation near a tunnel entrance," in *Proc. IEEE 65th Veh. Technol. Conf. (VTC-Spring)*, Apr. 2007, pp. 515–519.
[25] A. C. M. Austin, M. J. Neve, G. B. Rowe, and R. J. Pirkl, "Modeling the effects of nearby buildings on inter-floor radio-wave propagation," *IEEE Trans. Antennas Propag.*, vol. 57, no. 7, pp. 2155–2161, Jul. 2009.
[26] C. Guiffaut and K. Mahdjoubi, "A parallel FDTD algorithm using the MPI library," *IEEE Antennas Propag. Mag.*, vol. 43, no. 2, pp. 94–103, Apr. 2001.
[27] F. M. Pallares, F. J. P. Juan, and L. Juan-Llacer, "Analysis of path loss and delay spread at 900 MHz and 2.1 GHz while entering tunnels," *IEEE Trans. Veh. Technol.*, vol. 50, no. 3, pp. 767–776, May 2001.
[28] Z. Zhao, W. Hou, and J. Wang, "Effect of antenna location and polarization on radio wave propagation in tunnel," in *Proc. Int. Conf. Microw. Millim. Wave Technol. (ICMMT)*, May 2019, pp. 1–3.
[29] Z. Zhao and J. Wang, "Effect of antenna location on uniformity of radio wave coverage in rectangular tunnels with different cross section sizes," in *Proc. Int. Symp. Antenna Propag. (ISAP)*, Oct. 2019, pp. 1–3.
[30] C. S. Zhang and M. Yan, "Effects of cross section of mine tunnel on the propagation characteristics of UHF radio wave antennas," in *Proc. ISAPE*, Oct. 2006, pp. 1–5.

**ZHENYU ZHAO** was born in Shandong, China, in 1994. She received the B.E. degree from the School of Mechanical and Information Engineering, Shandong University, China, in 2016. She is currently pursuing the Ph.D. degree with the Institute of Lightwave Technology, Beijing Jiaotong University.

Her research interests include computational electromagnetics and radio wave coverage.

**JUNHONG WANG** (Senior Member, IEEE) was born in Jiangsu, China, in 1965. He received the B.S. and M.S. degrees in electrical engineering from the University of Electronic Science and Technology of China, Chengdu, China, in 1988 and 1991, respectively, and the Ph.D. degree in electrical engineering from Southwest Jiaotong University, Chengdu, in 1994. In 1995, he joined as the Faculty Member with the Department of Electrical Engineering, Beijing Jiaotong University, Beijing, China, where he became a Professor, in 1999. From January 1999 to June 2000, he was a Research Associate with the Department of Electrical Engineering, City University of Hong Kong, Kowloon Tong, Hong Kong. From July 2002 to July 2003, he was a Research Scientist with the Temasek Laboratories, National University of Singapore, Singapore. He is currently with the Key Laboratory of all Optical Network and Advanced Telecommunication Network, Ministry of Education of China, Beijing Jiaotong University, and also with the Institute of Lightwave Technology, Beijing Jiaotong University. His research interests include numerical methods, antennas, scattering, and leaky wave structures.

**WEIBIN HOU** was born in Hebei, China. He received the Ph.D. degree in electronic science and technology from Beijing Jiaotong University, Beijing, China, in 2019. From September 2017 to September 2018, he was a Visiting Student with the Department of Electrical and Computer Engineering, University of Toronto, Toronto, ON, Canada. He is currently working with the China Academy of Information and Communications Technology. His research interests include 5G wireless technology, antennas, and radio wave propagation. He received the Best Paper Award at MAPE 2015.